Biofabrication of Nanocellulose-Mycelium Hybrid Materials

Noam Attias, Michael Reid, Sylwia Carolina Mijowska, Illia Dobryden, Marcus Isaksson, Boaz Pokrov, Yasha I. Grobman, and Tiffany Abitbol*

Healthy material alternatives based on renewable resources and sustainable technologies have the potential to disrupt the environmentally damaging production and consumption practices established throughout the modern industrial era. In this study, a mycelium-nanocellulose biocomposite with hybrid properties is produced by the agitated liquid culture of a white-rot fungus (Trametes ochracea) with nanocellulose (NC) comprised as part of the culture media. Mycelial development proceeds via the formation of pellets, where NC is enriched in the pellets and depleted from the surrounding liquid media. Micrometer-scale NC elements become engulfed in mycelium, whereas it is hypothesized that the nanometer-scale fraction becomes integrated within the hyphal cell wall, such that all NC in the system is essentially surface-modified by mycelium. The NC confers mechanical strength to films processed from the biocomposite, whereas the mycelium screens typical cellulose-water interactions, giving fibrous slurries that dewater faster and films that exhibit significantly improved wet resistance in comparison to pure NC films. The mycelium-nanocellulose biocomposites are processable in the ways familiar to papermaking and are suggested for diverse applications, including packaging, filtration, and hygiene products.

1. Introduction

New materials based on renewable resources are needed to address pressing global material concerns. Two emerging forest-based materials, fungal mycelium and nanocellulose

N. Attias, Prof. Y. J. Grobman Faculty of Architecture and Town Planning Technion, Israel Institute of Technology Haifa 3200003, Israel

Department of Fibre and Polymer Technology KTH Royal Institute of Technology

Stockholm 10044, Sweden

Dr. S. C. Mijowska, Prof. B. Pokroy Department of Materials Science and Engineering

Technion, Israel Institute of Technology

Haifa 3200003, Israel

Dr. I. Dobryden

Department of Surface Science and Corrosion

KTH Royal Institute of Technology

Stockholm 10044, Sweden

M. Isaksson, Dr. T. Abitbol

RISE Research Institutes of Sweden

Stockholm 11428, Sweden

E-mail: tiffany.abitbol@ri.se



The ORCID identification number(s) for the author(s) of this article can be found under https://doi.org/10.1002/adsu.202000196.

DOI: 10.1002/adsu.202000196

(NC), are exceptionally promising as they can be processed into a versatile range of sustainable alternatives that include packaging, [1,2] flame-retardants, [3,4] and substitutes for meat and leather.^[5] The term nanocellulose encompasses the three main families of cellulosic nanomaterials, including cellulose nanocrystals (CNCs), cellulose nanofibrils (CNFs), and bacterial nanocellulose (BNC).[6] Here, the focus is on wood-based CNCs and CNFs, although these materials can be derived from other natural cellulose sources, including waste streams.[7] CNCs and CNFs are highly crystalline structural building blocks of the plant cell wall, with CNFs liberated by mechanical delamination and CNCs by chemical degradation.[8] CNCs are comparatively short and monodisperse (≈100 nm length and 5–10 nm width),^[9] whereas CNF sizes can vary significantly depending on pulp pretreatment and extent of fibrillation, with the finest grades usually produced from highly delaminated

chemically modified pulps, yielding fibrils with diameters of a few nm.^[10] NC's excellent mechanical properties and ability to form densely packed films make it attractive for composite reinforcement and barrier applications.[11,12]

From the millions of fungal species that exist, this study selected the white-rot basidiomycetes fungus Trametes ochracea, also known as Trametes multicolor. T. ochracea has been explored in previous works,[13,14] and was selected based on promising compatibility with NC observed in a prestudy evaluation that also included Trametes versicolor and Ganoderma sessile (unpublished solid-state incubations that showed comparatively uniform and healthy mycelium development with T. ochracea; Attias, Grobman, and Abitbol). T. ochracea, like most other fungi, forms continuous, filamentous multicellular structures called hyphae that branch, fuse, and extend to produce the complex 3D network known as mycelium. The fungal cell wall is composed of a dynamic^[15] and heterogeneous interwoven mesh of chitin, glucans, glycoproteins, and other polysaccharides, [16] creating interconnected layers, which together provide the properties required to withstand high internal hydraulic pressures, provide physical protection, and maintain internal humidity.[17] These properties play a key role when mycelium is employed as a structural biobased material.

In nature, white-rot fungi mycelium develops on wood, dispersing within and around it, preferentially decomposing lignin while leaving much of the cellulose intact.[18-20] Industrially, mycelium is commonly grown in submerged culture, forming www.advancedsciencenews.com

www.advsustainsys.com

2366/1486, 2021, 2. Downloaded from https://onlinelibrary.wiley.com/doi/10.1002/adsu.2020000196 by Epfl Library Bibliothèque, Wiley Online Library on [08/12/2024]. See the Terms and Conditions (https://onlinelibrary.wiley.com/rerms-and-conditions) on Wiley Online Library for rules of use; OA articles are governed by the applicable Creative Commons Licenses

macroscopic gelatinous hyphal aggregates, which are then processed to extract different microbial products.^[21] Depending on the culture conditions, the aggregates can develop into discrete pellets,^[22] with compositions and hyphal morphologies that are influenced by various interrelated factors, such as colony conditions, growth medium, agitation rate, and broth viscosity.^[21–23] Mycelium development is accompanied by the secretion of exopolysaccharides (EPS),^[24–26] and various proteins, including hydrophobins.^[27] White-rot fungi express lignocellulosic-degrading enzymes under specific conditions but the activity of these enzymes can be suppressed by the addition of easily digestible simple sugars or other nutrients into the growth medium.^[28,29]

In recent years, the role of white-rot fungi as nature's decomposer has been extended to the production of fungal-derived biocomposite materials.[30,31] Different fungal species, substrates, and approaches have been used to produce biocomposites with distinct properties. Space-filling composites produced from the solid-state cultivation of T. versicolor, T. ochrachea, or G. sessile with various substrates from agricultural waste presented different characteristics depending on the fungus-substrate combination.^[14] Pure mycelium sheets from the static liquid cultivation of Schizophyllum commune (wild-type or with hydrophobin gene deletion) were denser with hydrophobin gene deletion due to increased mucilage secretion and additionally material properties were affected by light and CO₂ levels.^[32] Films from G. lucidum or Pleurotus ostreatus were stiffer when grown from a feeding substrate composed of microcrystalline cellulose (MCC), compared to a mixture of MCC and easier to digest potato dextrose broth.[33] Nanopapers with tunable mechanical properties were obtained by processing together at different ratios the chitin- β -glucan complexes extracted from Agaricus bisporus (common white button mushroom) and Daedaleopsis confragosa fruiting bodies, which have distinct chitin to β -glucan ratios.^[34] Nanopapers produced from the chitinous extracts of various fungal species (T. versicolor, Allomyces arbuscula, and Mucor genevensis) were more hydrophobic due to a higher lipid content compared to nanopapers derived from A. bisporus.[35] Additional processing can be employed to further modify material properties, for instance, nanopapers produced from chitinous extracts treated with HCl or H2O2 (in addition to an initial alkaline extraction) became more hydrophilic, [35] and similarly, the mechanical properties of S. commune mycelial films were modified by impregnation with glycerol. [36]

Here, nanocellulose was uniformly dispersed within the *T. ochracea* growth medium, which was otherwise rich in available nutrients, including readily digestible glucose.^[28] Under these conditions, we were curious to understand if and how the presence of NC as a substrate influenced the properties of the resultant mycelium. NC has previously been combined with mycelium in postgrowth material processing,^[37] or in combination with fungal-derived chitin,^[38] but has yet to be used in the role of substrate. Mycelium-modified woodchips were bound together by CNFs to produce a material that was stiffer and more hydrophilic compared to a material produced from mycelium, woodchips, and CNFs, suggesting that coating the cellulosic substrate with mycelium can give improved material properties.^[37]

We report a fully biofabricated NC-mycelium hybrid, produced in a single step through an organic self-assembly process, where the NC becomes intimately enfolded within the mycelial network and is not simply added to the mycelium postgrowth. Here, the fungal mycelium is incubated alongside standard nutrients and NC (CNCs or CNFs) under agitated liquid culture conditions to produce a homogeneous NC-mycelium network structure with properties and composition dictated by the nature of the assembly and the extent of mycelium development. The results of this study point the way toward a family of different NC–mycelium biocomposites that are achievable by varying NC content and type, fungal species, growth conditions, and material processing and postprocessing approaches, leaving a rich terrain for follow-up works and the potential to tailor materials depending on the application of interest.

2. Results and Discussion

Hybrid NC–mycelium biocomposites were produced through the agitated liquid culture of *T. ochracea* containing different NC types (see Figure 1 for main NC types) added to the growth medium concomitantly with the fungal inoculation (co-incubation). CNCs and carboxymethylated CNFs present non-native sulfate half-ester and carboxymethyl functionalities, respectively. Carboxymethylated CNFs with different degrees of substitution (DS 0.1 and 0.3) and fibrillation (denoted by the number of passes through the microfluidizer, p) were used, as were enzymatically pretreated CNFs and bleached pulp fibers.

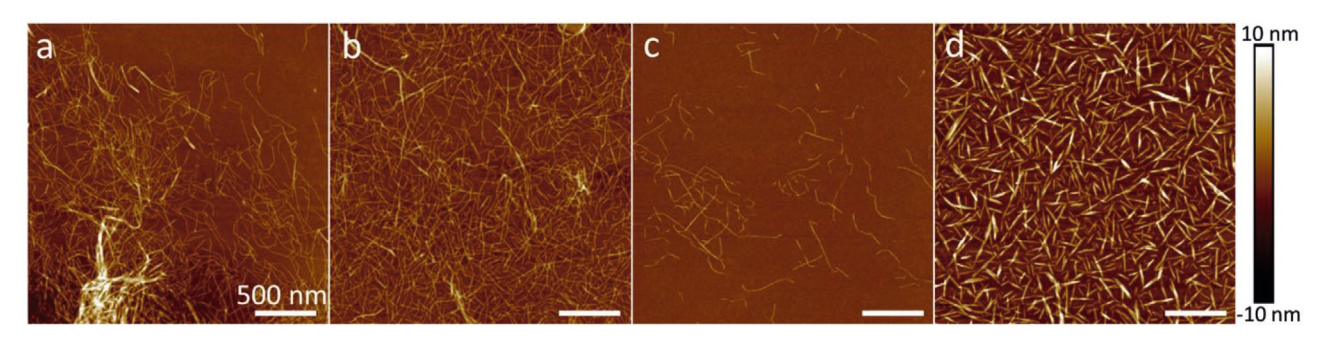


Figure 1. Atomic force microscopy (AFM) height images of main nanocellulose types used in this work: a) carboxymethylated CNF DS 0.1–1p, b) carboxymethylated CNF DS 0.1–4p, c) carboxymethylated CNF DS 0.3–4p, and d) cellulose nanocrystals. Carboxymethylated CNFs are denoted both by a degree of substitution (DS) and the number of passes (p) through the microfluidizer at 1700 bar.

www.advancedsciencenews.com www.advsustainsys.com

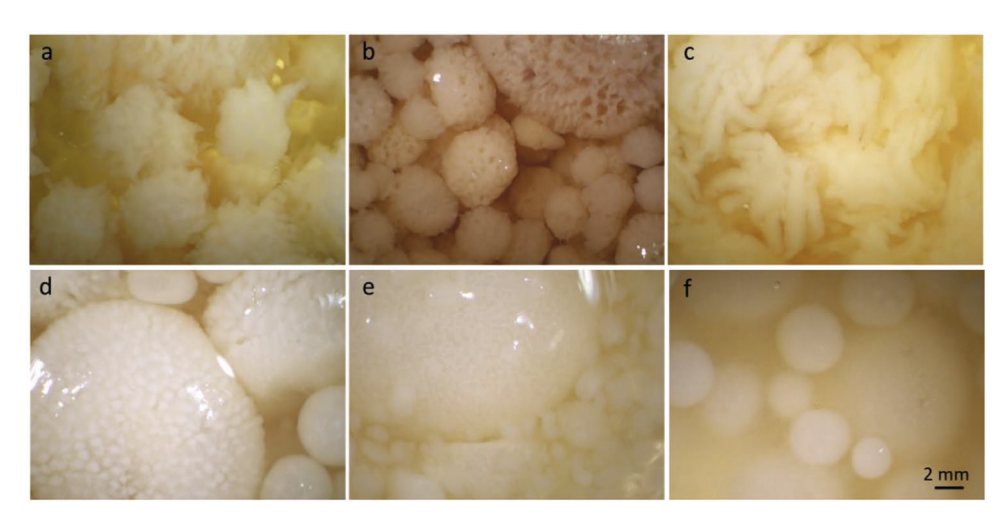


Figure 2. Stereomicroscope images of never-dried pellets showing different sizes and textures obtained through the co-incubation process, from round and smooth to rough with finger-like protrusions or sponge-like: a,b) pellets from *T. ochracea*, and co-incubations with c) 0.2% CNF DS 0.3–4p, d) 0.2% CNF DS 0.1–1p, e) 0.2% CNF DS 0.1–4p, and f) 0.5% CNF DS 0.1–1p.

Most incubations proceeded via the formation of pellets, multiplying over time and accompanied by a thickening of the surrounding liquid media due to EPS and protein secretion.^[32,39] The pellets were usually spherical, with diameters in the mm to cm range (see Figure 2 and Figure S1 in the Supporting Information), however, co-incubation with 2% CNC produced exceptionally small and oblong pellets (Figure S1, Supporting Information). Co-incubation with 2% carboxymethylated CNFs did not produce pellets, perhaps a result of the high viscosity of this sample restricting flow, such that mycelium development occurred at the air-liquid interface, with homogeneous development only occurring via manual agitation of the flask. Pellet size and appearance varied across samples, even among replicates, ranging from smooth textures to rough surfaces with finger-like protrusions, but were consistent within each incubation flask (Figure 2). The color, consistency, and morphology of the mycelial aggregates obtained by submerged culture are diverse and influenced by confounding factors, [19] however, some studies relate increasing broth viscosity and agitation speed to smaller pellet size.[22,23] Furthermore, variations in pellet morphology can be related to the employed processing conditions, for instance, crowded culture flasks and insufficient shaking may have limited homogeneous aeration and substrate mixing.

The first result of this work is that mycelium development occurred in the presence of NC (CNCs or CNFs), an aspect that was not taken for granted. Further, the microscopic

appearance of the hyphae within the pellets seemed surprisingly influenced by the NC content, although this observation can also be consistent with the natural variation observed in the pellets (Figure 2). High resolution-scanning electron microscopy (HR-SEM) of the pellets (Figure 3) show ≈2 µm diameter branched and irregular hyphae for T. ochracea, covered in places by a fine web of EPS (Figure 3a), whereas the hyphae became less branched and more regular with the addition of NC (Figure 3b,c). Increasing the CNF content in the growth medium from 0.25% to 2% (Figure 3b,c) also produces hyphae with $\approx 2 \mu m$ diameters but their morphology was dramatically altered to smooth, continuous, and spaghetti-like, with fewer clear junctions, although, as mentioned, this effect may not necessarily be related to the presence of NC and warrants further study. Hyphae with typical dimensions are obtained from co-incubation with CNCs but HR-SEM visualization was dominated by nm-scale fibrillar features, which were also seen in other samples, but to a lesser extent (see Figure S2 in the Supporting Information). The differences in hyphae appearance may be related to presence of NC, perhaps through a specific interaction between NC and mycelium or through indirect factors, such as the viscosifying effect of NC and consequent hindrances to mass transport. Substrate type, nutrient profile, and growth conditions can all influence hyphal appearance and properties,[22,40,41] making it difficult to pinpoint the precise origin of the variation.

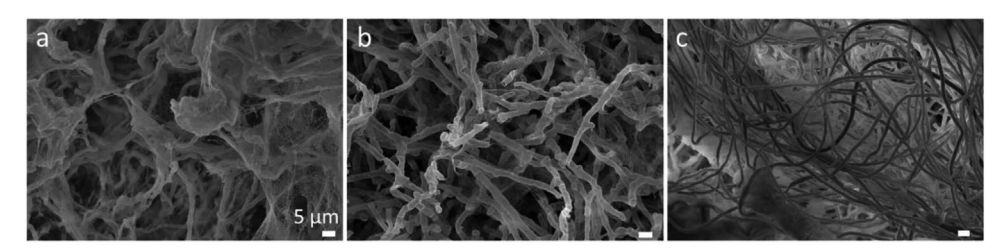


Figure 3. HR-SEM of a) pellets after critical point drying showing interior of pellet from T. ochracea, and pellets from co-incubation with b) 0.2% CNF DS 0.1–1p and c) 2% CNF DS 0.1–1p. All scale bars = 5 μ m.

23667484, 2021, 2, Dwnbabded from https://onlinelblarg.w.iely.com/doi/10,1002/adsu.202000196 by Epf1 Library Bibiohèqee, Wiley Online Library on (08/12/2024). See the Terms and Conditions (https://onlinelbbrary.wiely.com/rems-and-conditions) on Wiley Online Library from less of use; OA articles are governed by the applicable Creative Commons Licenses

www.advancedsciencenews.com

www.advsustainsvs.com

Table 1. Mass balance for *T. ochracea* and NC–mycelium hybrid biocomposites produced by co-incubation with carboxymethylated CNFs (DS 0.1–1p), CNCs, enzymatic CNFs (Enz-CNF), and pulp fibers. The total solids per incubation was determined from mixtures that were autoclaved, dialyzed, and homogenized.

	Total solids [g]	NC mass [g]	Mycelial mass [g]	NC content [%]	Mycelial content [%]
T. ochracea	2.1	0	2.1	0	100
+0.25% carboxy-CNF	4.8	1.5	3.3	31	69
+0.25% carboxy-CNF (repeat)	6.2	1.5	4.7	24	76
+0.5% carboxy-CNF	6.1	3	3.1	50	50
+0.25% CNC	3.6	1.5	2.1	42	58
+0.25% Enz-CNF	3.8	1.5	2.3	39	61
+0.25% pulp fibers	3.2	1.5	1.7	46	54

The effect of cellulose type on the yield of the mycelium obtained from the different fermentations was studied. The solid yield of mycelial mass (hyphae + secreted matter) was determined gravimetrically as the dry content of the homogenized fermentations, subtracted by the mass of cellulose added to the fermentation. The mass balance results presented in Table 1 intriguingly suggest that the presence of carboxymethylated CNFs encourages the formation of mycelial mass. The reasons for this apparent increase in yield may be related to the digestion of carboxymethylated CNFs or of noncrystalline carboxymethylated chains at the modified CNF surfaces. Another possibility is that carboxymethylated CNFs associate to the hyphal cell wall in such a way as to interfere with EPS production due to mass transport constraints, allowing more resources to be diverted toward the production of mycelium. However, as CNCs, enzymatic CNFs, and pulp fibers do not seem to have the same impact on mycelial development, the subsequent text and discussion mainly focus on the carboxymethylated CNF hybrid, with an aim of understanding how this CNF type associates with mycelium. Finally, we note that the CNF content listed in Table 3 and in the description of hybrid materials assumes that the CNF is not digested in the co-incubation process.

Various analyses were conducted to localize the NC within the mycelium and to understand the influence of NC on the biocomposite properties. Polarized optical microscopy (POM) was used to distinguish between hyphae, which are not birefringent, and NC, which is birefringent. In this way, POM can

be used to identify larger nanocellulose fragments as well as assemblies of nanoscale elements. POM of pure T. ochracea pellets showed a fine but nonbirefringent hyphal network structure, whereas pellets from NC-mycelium co-incubations showed birefringent features due to the presence of NC (Figure 4). Remarkably, no birefringence was detected in the surrounding liquid media of the NC containing samples (see Figure S3 in the Supporting Information for POM of the postgrowth liquid media and initial NC suspensions). Partially fibrillated um-scale carboxymethylated CNF fragments appear to be engulfed by hyphae (Figure 5). Further, Figure 5a and Figure S4 in the Supporting Information highlight that for carboxymethylated CNFs, both distinct um-scale fibrils and assemblies of nm-scale fibrils become fully integrated within the hyphal network, with no CNFs evidenced outside the cohesive mass generated via the co-incubation process. Similar results were observed for co-incubation with enzymatic CNF and pulp fibers, which showed mycelium growing on and around the cellulosic substrates (see POM in Figure S5 in the Supporting Information). Overall, observations by POM and HR-SEM are consistent with NC accumulating and dispersing within the mycelium pellets and being depleted or absent from the surrounding media. Large NC fibrils (and pulp fibers) seem to act as a scaffold for mycelium growth, in ways similar to other macroscopic cellulosic substrates (e.g., woodchips, saw dust), however, how the substantial nm-scale fraction of NC interacts and associates with the mycelium is not yet addressed.

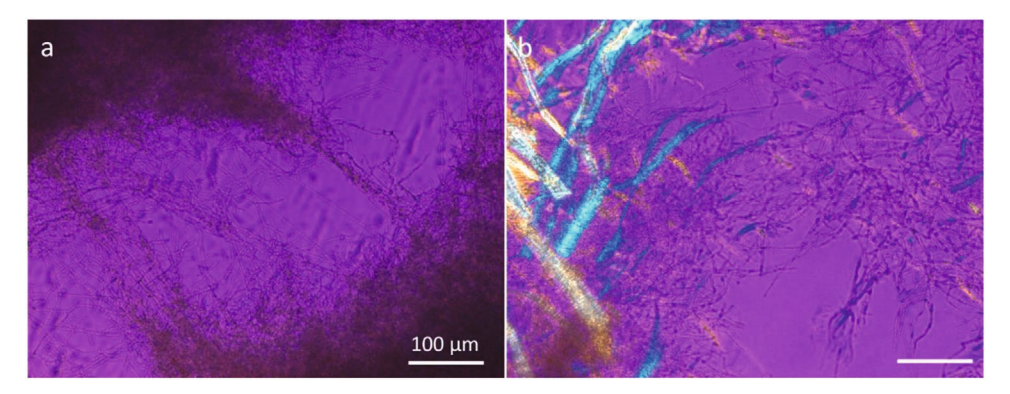


Figure 4. POM of pellets pressed between a glass slide and coverslip: a) pellet from T. ochracea and b) pellets from co-incubation with 0.5% carboxymethylated CNF DS 0.1–1p. Both scale bars = $100 \, \mu m$.

and-conditions) on Wiley Online Library for rules of use; OA articles are governed by the applicable Creative Commons-

Figure 5. a) POM of 0.2% carboxymethylated CNF DS 0.1–1p pellet compressed between a glass slide and coverslip and b) HR-SEM of the same pellet after CPD. Both scale bars = $20 \, \mu m$.

Attenuated total reflectance-Fourier transform infrared (ATR-FTIR) spectroscopy presented in **Figure 6** probes the surfaces of films at a μ m-scale depth of penetration. The films were prepared by vacuum filtration of the fibrous slurry obtained by homogenization of the liquid fermentations after dialysis. The hybrid film has mycelium-derived bands that do not occur in the carboxymethylated CNF film, most notably bands at 1640 and 1540 cm⁻¹, assigned to protein, and a band at 1370 cm⁻¹, assigned to chitin, and the bands at 3300–2850 cm⁻¹ are more pronounced in mycelium-containing films due to the presence of lipids.^[42] It is difficult to identify entirely cellulose-derived bands in the hybrid film, which contains other carbohydrates, such as β -glucans, which have a chemical signature that overlaps with the CNFs (CNFs are a sort of β -glucan).

Nanoscale surface analyses by X-ray photoelectron spectroscopy (XPS) of freeze-dried pellets (exterior surfaces and interior surfaces exposed by fracture), a pure carboxymethylated CNF aerogel, and films produced by vacuum filtration are presented

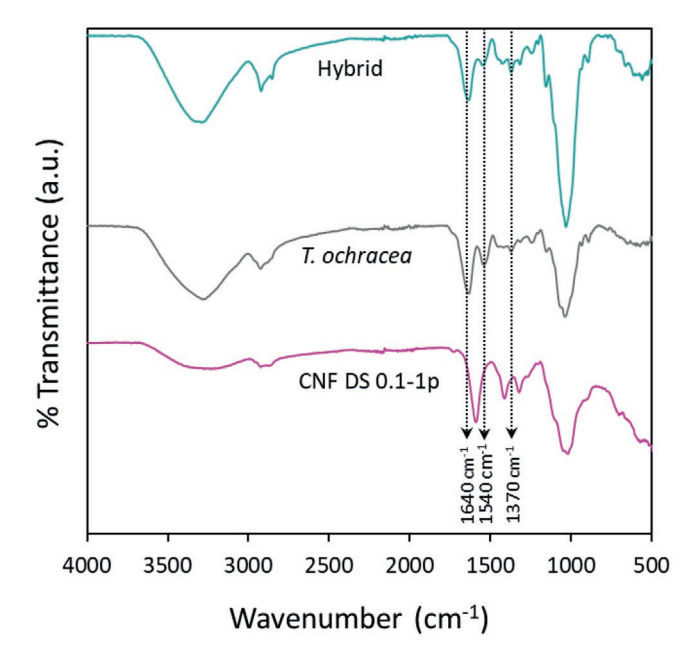


Figure 6. ATR-FTIR of various films including a CNF–mycelium biocomposite hybrid produced by co-incubation with carboxymethylated CNF. Hybrid was produced by the co-incubation of mycelium with 0.2% CNF DS 0.1–1p to give materials with a $\approx\!30\%$ CNF dry content.

in Table 2. As the CNFs do not contain nitrogen, all detected nitrogen was attributed to chitin or other nitrogen containing species in the mycelium. The dilution of mycelium with NC was expected to manifest in higher O/C and lower N/C ratios for the NC-mycelium hybrids compared to pure T. ochracea, however, XPS ratios were similar, with O/C ratios of 0.59-0.65 and N/C ratios of 0.01-0.04 for the pellets, and 0.48-0.49 and 0.05-0.06, respectively, for the films. The difference in O/C and N/C ratios between the biocomposite pellets and films may be related to different compositions in the films, which were processed from the complete mixture of pellets and surrounding media postdialysis. As the XPS measurements probe a depth of ≈10 nm at a lateral resolution of ≈1 mm², the similar values obtained whether CNFs were present or not, supports the hypothesis that the CNFs become fully engulfed by mycelium during the fermentation process. The pure CNF aerogel had an O/C ratio that coincided with the theoretical value expected for cellulose, however, all samples presented minimal and unavoidable C1 contributions and the O/C for the CNF sample is expected to further deviate due to carboxymethyl surface groups (see Figure S6 in the Supporting Information for representative survey scans and high-resolution carbon spectra). Taken together, the surface analyses presented in Figure 6 and Table 2 indicate that compositionally similar qualities of mycelium are produced whether carboxymethylated CNFs are included in the incubation or not, and that the mycelium signature is generally more prominent at the surface of the hybrids, including interior surfaces.

Table 2. XPS surface analysis of dialyzed and freeze-dried co-incubation pellets, vacuum-filtered films made from dialyzed and homogenized pellets and media, and control CNF aerogel. In all instances, carboxymethylated CNF DS 0.1–1p and ≈30% CNF dry content.

O/CN/C	Pellet interior	Pellet exterior	Surface
T. ochracea	0.59	0.65	0.48 ^{a)}
	0.01	0.04	
			0.05a)
Carboxy-CNF + T. ochracea	0.65	0.61	0.49a)
	0.02	0.03	
			$0.06^{a)}$
Carboxy-CNF	-	_	0.83 ^{b)}

^{a)}Films; ^{b)}Aerogel.

23667486, 2021, 2, Downloaded from https://onlinelibrary.wiley.com/doi/10.1002/adsu.202000196 by Epfl Library Bibliothèque, Wiley Online Library on [08/12/2024]. See the Terms and Conditions (https://onlinelibrary.wiley.com/term

-and-conditions) on Wiley Online Library for rules of use; OA articles are governed by the applicable Creative Commons I

www.advancedsciencenews.com

www.advsustainsys.com

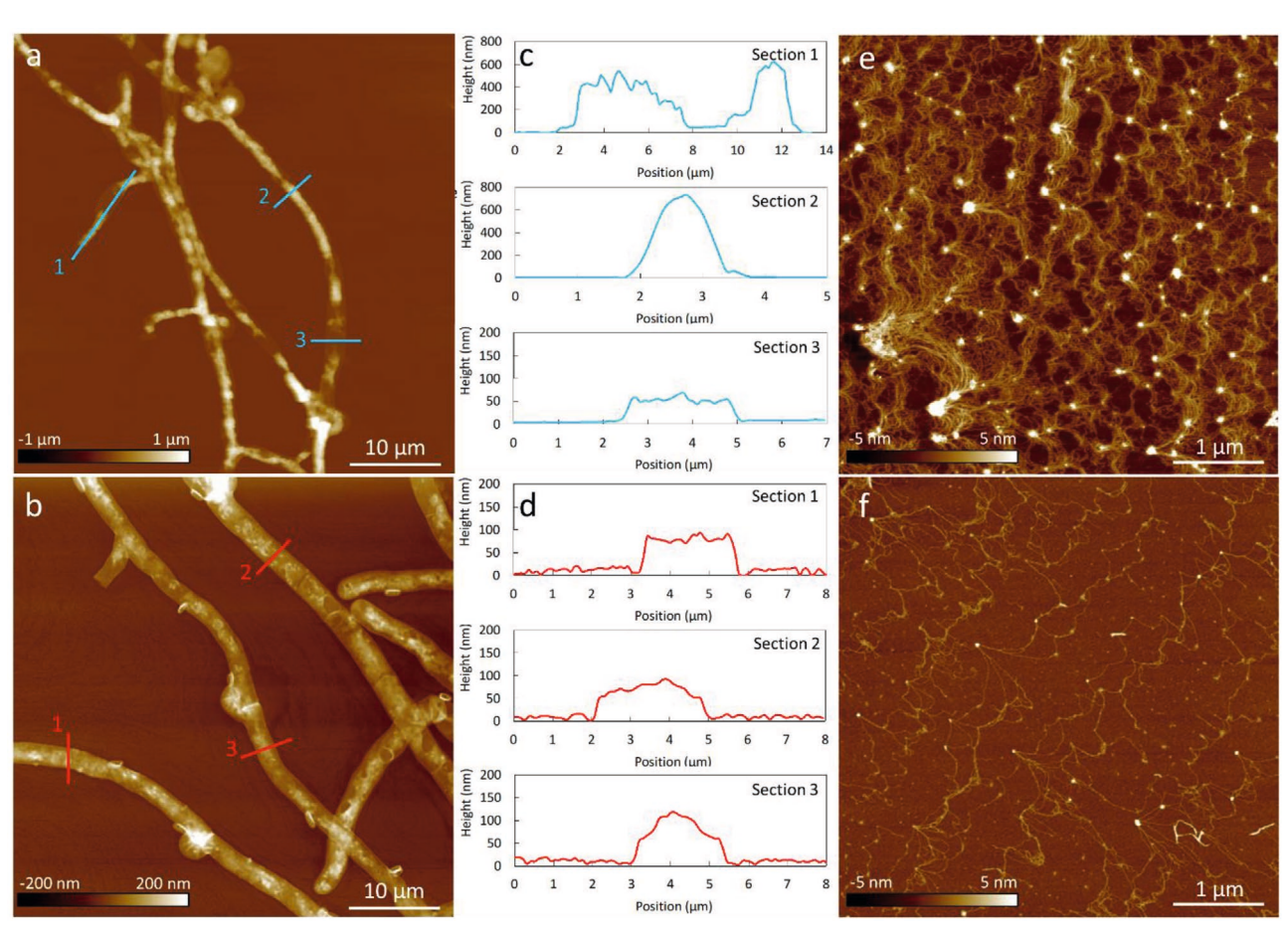


Figure 7. Large-scale AFM height images (50 μm), associated sections, and small-scale AFM height images (2.5 μm), respectively, for a,c,e) *T. ochracea* and b,d,f) 0.2% carboxymethylated CNF DS 0.1–1p biocomposite hybrid.

Nanoscale imaging by atomic force microscopy (AFM) provided further insights on the localization of NC and its influence on hyphal morphology. AFM images of homogenized mycelial mass (pellets + surrounding media, postdialysis) are shown in Figure 7. T. ochracea and a carboxymethylated CNFmycelium hybrid (Figure 7a,b), respectively, show the typical branched hyphal network, with some homogenization-induced breakages and hyphae widths of $\approx 2-3 \mu m$. Sections along the *T*. ochracea hyphae (Figure 7c) presented low and high features, up to ≈600 nm, whereas the CNF-mycelium hybrid was distinctly more uniform with a collapsed-hyphal height of ≈100 nm (Figure 7d). This observation of more uniform morphologies for the CNF-mycelium biocomposites compared to T. ochracea is generally consistent with the HR-SEM presented in Figure 3. Closer inspection of the seemingly empty spaces in Figure 7a,b indicate that these regions are populated with a network of fine EPS, with heights of ≈1–3 nm (see Figure 7e,f), consistent with previously published AFM images of fungal glucans.^[43]

Three features stand out from the AFM: 1) CNF is absent from the areas around the hyphae, 2) EPS content appears to be higher in pure *T. ochracea* compared with the CNF–mycelium hybrid, and 3) the hyphae of the NC–mycelium hybrid dry to a more collapsed state. The first observation reinforces and extends the POM data (Figure 4; Figures S4 and S5, Supporting Information), where the CNFs were only seen in close

association to the mycelial network, but did not conclusively preclude nm-scale CNFs, too small to be visualized by optical microscopy, from being excluded from the mycelial network, whereas AFM analyses demonstrates the absence of a nanofraction in surrounding medium. These nm-scale CNF fractions, which constitute a significant proportion of the CNFs, are easily visualized by AFM, and yet were not observed in the areas surrounding the hyphae, perhaps suggesting that they are somehow integrated within the hyphal cell wall, which is built up in part of chemically similar glucans. Indeed, a close-up by AFM of a CNC-mycelium hybrid hyphae (Figure 8) shows nanocrystalline elements, apparently integrated within the external hyphal cell wall, and no CNC discernible outside of the hyphae. (Similar images were obtained for a carboxymethylated CNF-mycelium hybrid, but CNFs were less clearly visualized perhaps as their nanofraction is less rigid and thinner than CNC.)

The second AFM observation of an apparently denser EPS network in pure *T. ochracea* (Figure 7e) is supported by the HR-SEM images of the pellets (Figure 3), where a fine intracellular EPS mesh covers the *T. ochracea* hyphae but is less pronounced in the hybrid pellets. As mentioned in the introduction, similar to pellet formation,^[23] EPS formation depends on many incubation-related factors, including substrate content (carbon and nitrogen sources), temperature, pH, and incubation duration.^[24–26] EPS can be consumed in the later stages of

23667486, 2021, 2, Dwnholoded from https://onlinelibrary.wiley.com/doi/10.1002/adsu.202000196 by Epfl Library Bibliothèque, Wiley Online Library on [08/12/2024]. See the Terms and Conditions (https://oinleilibrary.wiley.com/erms-and-conditions) on Wiley Online Library for rules of use; OA archies are governed by the applicable Creative Conditions.

Figure 8. a) AFM height and b) amplitude images of a hyphae produced from the co-incubation of 2% CNC with T. ochracea.

fungal growth as a strategy to accumulate carbon and mass, $^{[24]}$ but at the same time EPS secretion is hindered by denser hyphal cell walls. $^{[26]}$

Cryo-SEM observation and nanoindentation measurements were conducted to clarify the hyphae height variation measured by AFM, where the hybrid biocomposite hyphae appeared uniformly flat upon drying, in contrast to the *T. ochracea* hyphae that presented flat regions and elevated regions attributed to various organelles within the cells (see Figure 7). Cryo-SEM showed typical organelle structures within the hyphae of pure *T. ochracea* and the hybrid biocomposite (see Figure S7 in the Supporting Information), perhaps indicating that differences in cell wall properties are responsible for variations upon drying. The apparently diminished EPS content in the biocomposite hybrid may then reflect cell wall densification that occurs in the co-incubation with CNFs, which also causes the hybrid hyphae to collapse on drying to flat ribbon-like shapes (see Figure 7).

The surface roughness and elastic modulus of a hybrid biocomposite film (\approx 30% carboxymethylated CNF dry content) compared to a pure *T. ochracea* film are presented in **Table 3**. Topography images associated with the roughness measurements are presented in Figure S8 in the Supporting Information and nanomechanical mapping images in Figure S9 in the Supporting Information. At the μ m-scale, the CNF-mycelium biocomposite is less rough, an observation that is consistent with images presented in Figures 3 and 7, which generally show that more uniform hyphae, with fewer height variations, are obtained by the co-incubation of mycelium with CNFs, a feature that seems to translate into smoother films. The difference in roughness is minimized as the scan area is decreased, consistent with fewer hyphal junctions included within the

scan area, and indeed at the nm-scale (300 \times 300 nm scan), the roughness values are similar between samples. The elastic modulus maps, shown in Figure S8 in the Supporting Information, demonstrate local property variation over the scan areas of stiffer and softer areas. Nanoindentation results indicate that the elastic modulus of the carboxymethylated CNF-mycelium biocomposite film is reinforced by 44% compared to the pure *T*. ochracea film. Finally, the relatively low standard deviation associated with the elastic modulus of the CNF-containing hybrid may reflect an overall compositional uniformity and the homogeneous distribution of NC. A possible reason for the increased modulus and other AFM observations is that carboxymethylated CNF become integrated within the cell wall of the mycelium, densifying and stiffening its structure. Then, the hybrid cell wall yields a more uniformly collapsed structure upon drying, whereas the pure T. ochracea cell wall, in the absence of NC reinforcement, is less rigid (and perhaps thinner) and better able to conform to the shape of the underlying organelles. Furthermore, the stiffer hyphal cell wall may be responsible for the apparent uniformity of the hybrid hyphae (see HR-SEM in Figure 3), which present fewer buckled and kinked features compared to the pure mycelium.

Bulk properties of films produced were also probed to better contextualize the apparent association between carboxymethylated CNFs and mycelium that occurs in the co-incubation. The dewatering rate to produce the hybrid films was observed to be significantly hastened, from the hours needed for pure carboxymethylated CNFs, to minutes for the hybrid materials. The slow drainage of CNFs (due to their high affinity to water) is a serious hindrance to the roll-to-roll processing of CNF materials (and NC materials in general), which then necessitates

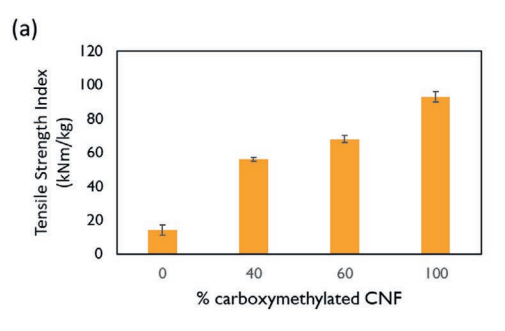
Table 3. Film roughness at different size scales and elastic modulus by nanomechanical mapping. The elastic modulus was measured and evaluated for at least five different locations for each sample to obtain the average value. Carboxymethylated CNF–mycelium biocomposite has a CNF dry content of ≈30%.

	$10 \times 10 \mu m$, R_a [nm]	$5 \times 5 \ \mu m, \ R_a \ [nm]$	$0.3 \times 0.3 \ \mu m, \ R_a \ [nm]$	Elastic modulus [GPa]
T. ochracea	268	110	1.9	1.6 ± 0.6
CNF + T. ochracea	135	53	3	2.3 ± 0.2

2366/1486, 2021, 2. Downloaded from https://onlinelibrary.wiley.com/doi/10.1002/adsu.202000196 by Epf1 Library Bibliothèque, Wiley Online Library on [08/12/024]. See the Terms and Conditions (https://onlinelibrary.wiley.com/rems-and-conditions) on Wiley Online Library for rules of use; OA aristles are governed by the applicable Creative Commons Licenses

www.advancedsciencenews.com

www.advsustainsys.com



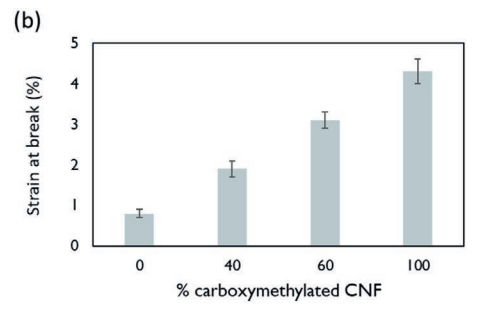


Figure 9. a) Tensile strength index and b) strain at break of hybrid films from the co-incubation of carboxymethylated CNF and mycelium compared to a pure mycelium film and a pure CNF film. Film grammage is 30 g m $^{-2}$ and results are an average of six measurements with associated standard deviations as the error bars.

expensive and customized drying strategies. The equilibrium water uptake of the hybrid films (up to 60% CNF content) was similar to pure *T. ochracea* films at \approx 2 g g⁻¹ compared with \approx 12 g g⁻¹ film for pure carboxymethylated CNF films. Furthermore, hybrid films remain fully intact in water even after very long immersion times of >1 year, whereas the carboxymethylated CNF films quickly form hydrogels with no appreciable wet strength. Finally, bulk tensile film properties of the hybrid carboxymethylated CNF films (compared to a pure CNF films and to a pure *T. ochracea* film) were evaluated and are presented in **Figure 9**. Here, a linear increase in tensile properties is observed with increasing CNF content in the hybrid.

At the heart of the discussion is the fate of the nanofraction of the carboxymethylated CNFs, which has evaded our attempts at direct localization and visualization. Is this nanofraction digested or does it become part of the hyphal cell wall? At the micrometer-scale by optical microscopy, the CNFs that participated in the co-incubation appear hairy, covered by mycelium. Compositional surface analyses confirm this picture of CNFs surface-modified by mycelium since they only detect mycelium. Free water uptake of hybrid films also shows mycelium-like behavior, further supporting that cellulose surfaces are covered by mycelium. The appearance of the hyphae also seems to be influenced by the presence of the CNFs, and the hyphal morphology upon drying supports a stiffer cell wall in the hybrid, as does the elastic modulus measurements, which show a stiffness increase of ≈44% for a hybrid that contains 30% CNFs. Similarly, bulk tensile measurements indicate a linear increase in tensile properties with CNF content in the hybrid films.

Based on these data, it is our hypothesis that the nanofraction of the carboxymethylated CNFs become integrated into the cell wall of the hyphae, without being digested, particularly considering the linear increase in bulk tensile properties, which is derived from the nanocellulose component, and would be entirely unexpected if the CNFs were degraded to a serious extent. (Note, noncrystalline carboxymethyl-modified surface chains may be digested, but the yield increase with carboxymethyl cellulose is generally attributed to the mechanical reinforcement and densification of the cell wall.) The surface-modification of the CNFs by mycelium, with the CNFs remaining intact, confers interesting properties, such as reduced moisture sensitivity (i.e., free swelling in water, drainage rate) compared to pure CNF materials, while retaining the strengthening aspect of the CNFs. The coverage of the CNFs by mycelium is

a promising and nontraditional surface modification approach that may be useful for the reinforcement of mycelium and mycelium-modified materials, while minimizing interfacial mismatch.

The nature of the interaction between the fungi and nanocellulose (especially the types with non-native surface functionalities) is not fully clear. White-rot fungi, such as T. ochracea, are known for their ability to bind metal ions from the environment, a trait that is widely utilized for bioremediation, [44,45] but also for the in situ growth of metal and mineral ions into nanostructures.[46–48] The interactions between the ions and the mycelium is apparently electrostatic, with positively charged ions binding to negative surface sites in the cell wall and associated EPS, but as the NC used is negatively charged (or basically uncharged for enzymatic CNFs and pulp fibers), and furthermore, as charge effects are likely screened due to the high electrolyte content of the growth media, electrostatics are probably not the main factor in the current work. Instead, the interactions between NC and mycelium may be mediated by other binding interactions, perhaps the same interactions that bind mycelium to cellulose substrates in general, for instance, fungi can bind to cellulose via carbohydrate binding modules (CBMs).[49,50] Previous studies have used the interactions between CBMs and cellulose to bind specific recombinant proteins to CNCs via a CBM, producing CNC-protein hybrid materials.^[51–53] In the current study, NC becomes covered with mycelium during co-incubation, with the nanofraction hypothesized to be interwoven within the polysaccharide layers of the external hyphal cell wall and larger fibril fragments covered in mycelium fuzz, similar to what occurs with other micro or macrosubstrates, such as saw dust, woodchips, and pulp fibers. We suggest that the mycelium binds both the CNF nanofraction and larger (less fibrillated) CNF elements like the way that it binds other wood substrates, with the difference being one of perspective related to the sizes of the different wood elements relative to the hyphae.

The co-incubation approach used in this work proceeded via the production of mycelium pellets surrounded by a polysaccharide-rich broth, where the composition and overall yield of the biocomposite seems to be influenced by the presence of NC, and where NC was found to be concentrated within the hyphal cells and depleted from the liquid media surrounding the pellets. In this way, a nature-directed self-assembled biocomposite comprising NC and mycelium intimately integrated

23674848, 2021, 2, Dwnholaded from https://onlinelibrary.wisey.com/doi/10.1002/adsu.202000196 by Epfl Library Biblothèque, Wiley Online Library on (08/12/2024). See the Terms and Conditions (thps://onlinelibrary.wisey.com/terms-and-conditions) on Wiley Online Library for rules of use; OA articles are governed by the applicable Creative Commons Licenses

www.advancedsciencenews.com www.advsustainsys.com









Figure 10. Summary of the biofabrication process of hybrid biocomposites from mycelium and NC based on the incubation of mycelium culture discs in a nutrient-rich liquid media containing NC. Photographs from left: a) mycelium–NC pellets in liquid culture at the end of incubation, b) homogenized mycelium–NC hybrid biocomposite fibrous slurry, c) films (d = 8 cm) produced by vacuum filtration of homogenized mixtures, and d) aerogels (d = 4 cm) processed from the same mixtures.

into what is effectively a single cohesive material was obtained. After dialysis and homogenization, the biocomposite consisted of a uniform liquid mass comprised of a mycelium-modified NC network (see Figures 4b and Figure S4 in the Supporting Information, POM), which resisted dilution, undergoing phase separation upon dilution, with a water phase forming above the diluted material. This effect was captured for the carboxymethylated CNF samples by turbidity measurements as a function of time for undiluted hybrids at native solid contents of 0.41-0.96 wt% and for samples diluted to 0.1 wt% (Figure S10, Supporting Information). The undiluted biocomposites remain stable as a function of time (Figure S9a, Supporting Information), whereas the diluted biocomposites (Figure S9b, Supporting Information) exhibit an increase in absorbance at 550 nm with time due to sample phase separation, yielding an upper water phase and a lower, densified phase.

Significantly, many previously described mycelium-based biocomposites combine fungal inoculum with solid biomass, such as woodchips or saw dust,[14,54,55] whereas the current approach, which introduces the biomass in the form of a nanoscale colloidal particle, has the advantage of producing a versatile liquid mass. This can be used as-is, for instance, to be dried into films or aerogels (see Figure 10), or 3D printed or dried into coatings, for instance, to impart wet resistance, but can also potentially be processed together with macroscale solid biomass to give a more traditional, space-filling mycelium biocomposite, strengthened by the inclusion of mycelium-modified NC. Detailed characterization of the materials presented in Figure 10 is beyond the scope of the current manuscript but is planned for a separate upcoming work that considers wettability, mechanical properties, and barrier properties, to evaluate how the nature of the biocomposite assembly informs material properties.

3. Conclusion

The liquid culture co-incubation of *T. ochracea* mycelium together with nanocellulose gives a cohesive and uniform biocomposite material, where the nanocellulose becomes covered by mycelium, and with evidence that suggests that nm-scale carboxymethylated cellulose nanofibrils become integrated within the hyphal cell walls. Co-incubation of mycelium with carboxymethylated CNF seems to influence the morphology of the hyphae, which apparently become more fibrillar, regular,

stiffer, and flatter upon drying to give uniform ribbon-like collapsed tubes. The balance of nanocellulose, mycelium, and associated polysaccharides within the biocomposites is governed by nature, with data that suggest that mycelial mass is enhanced and EPS content diminished by co-incubation with carboxymethylated CNFs. The organic approach presented in this work unifies two disparate materials into a single material that can be easily processed into different forms, such as films and aerogels, giving materials with versatile potential utility, for instance, in paper and board applications, such as printing and packaging, which can benefit from improved wet resistance in conjunction with nanocellulose strengthening effects.

4. Experimental Section

Materials: T. ochracea culture was purchased from Mycelia nv (Belgium) and stored at 4 °C. The following list of standard reagents required for the fungal growth media were purchased from Sigma-Aldrich: D-glucose, peptone, yeast extract, malt extract, KH₂PO₄, K₂HPO₄, and MgSO₄. Other standard reagents and materials were also purchased from Sigma-Aldrich: NaOH, monochloric acetic acid, ethanol, isopropanol, methanol, sodium hydrogen carbonate, polyallylamine hydrochloride (PAH), and regenerated cellulose dialysis membranes (76 mm, 12–14 kDa MW cut-off). Commercial spray dried CNC from the sulfuric acid hydrolysis of bleached softwood was purchased from CelluForce. Never-dried bleached softwood pulp from Domjsö-MORE (Dissolving Pulp Plus) was used as the cellulose source for the different CNF grades. The monocomponent endoglucanases (FiberCare) used to pretreat the pulp for the enzymatic grade CNFs was obtained from Novozymes.

NC Processing and Production: i) Spray-dried CNC powder was combined with Milli-Q water to 2% consistency by overhead mixing, followed by probe sonication at 5000 J g⁻¹, and vacuum filtration (Munktell 3). This CNC grade had been thoroughly characterized in the literature and had a surface charge from sulfate half-ester groups of $\approx\!250~\mu\text{eg}~g^{-1}.^{[9]}$ ii) Carboxymethylated CNFs were produced according to the method described in 2008 by Wågberg et al. $^{[56]}$ to obtain a suspension with a DS of 0.1, or equivalently $\approx\!600~\mu\text{eg}~g^{-1}$, with DS defined in Equation (1)

$$\frac{\text{AGUMW (160 g mol}^{-1})}{\left[\frac{1}{\text{Total charge}} - \text{CH}_3\text{COONa MW (80 g mol}^{-1})\right]}$$
(1)

where AGU stands for anhydroglucose unit and total charge is measured by the titration of an acidified suspension with sodium hydroxide. To achieve CNFs from the carboxymethylated pulp, the material was homogenized at 1700 bar (Microfluidizer M-110EH, Microfluidics Corp.,

ADVANCED SUST AINABLE SYSTEMS

23674848, 2021, 2, Dwnholaded from https://onlinelibrary.wisey.com/doi/10.1002/adsu.202000196 by Epfl Library Biblothèque, Wiley Online Library on (08/12/2024). See the Terms and Conditions (thps://onlinelibrary.wisey.com/terms-and-conditions) on Wiley Online Library for rules of use; OA articles are governed by the applicable Creative Commons Licenses

www.advancedsciencenews.com www.advsustainsys.com

US, 200 μ m \times 100 μ m chamber) with 1 pass (1p) through the homogenizer or 4 passes (4p) for a finer grade. The DS 0.3 carboxymethylated CNF (\approx 1700 μ eg g $^{-1}$) used in this work was prepared in the same fashion as the DS 0.1 CNFs with the following modifications: a 4.4× increase in monochloric acetic acid content and 2.7× increase in sodium hydroxide. iii) Enzymatically pretreated CNFs were produced from Dissolving Plus pulp (Domsjö-More) treated with a monocomponent endoglucanase, as has been described in detail elsewhere, [57] followed by 10 passes through the microfluidizer at 1700 bar. The enzymatic CNFs have a low negative total charge of \approx 30 μ eg g $^{-1}$.

NC Nanoyield: Approximate nanoyields of the NC samples were measured by high-speed centrifugation of dilute suspensions ($1000 \times g$, 20 min, 0.02 wt%, 1 L volume, divided). Comparison of the solid content of the supernatant, containing the nm-scale NC, to the total solid content of the initial suspension, gives the nanoyield (%). As described, the nanoyield of DS 0.1-1p CNFs is approximately 25%, with higher values obtained for finer CNF grades and 100% for the CNCs.

Mycelium Cultures: T. ochracea was maintained in Petri dishes (85 mm diameter) containing malt-agar. The malt-agar contained: agar (15 g), peptone (10 g), and malt extract (30 g), dissolved in deionized water (1 L). $^{[46]}$

Fungal Culture Conditions: For the pure T. ochracea culture, the following medium was used, as has been previously detailed by Livne et al.: D-glucose (15 g), peptone (2.5 g), yeast extract (3 g), KH₂PO₄ (1 g), K₂HPO₄ (0.2 g), and MgSO₄ (0.5 g) dissolved in 1 L deionized water and adjusted to pH 5.5. [46] 8 mycelium disks (6 mm diameter) cut from malt agar plates were used as inoculum for the incubations that were conducted in 1 L flask containing 600 mL medium for 14 d under controlled conditions (50% RH, 23 °C), in the dark, with continuous shaking at 120 rpm. To terminate the mycelium growth, the mixtures were autoclaved (121 °C, 1 h). The pH after incubation and autoclave was observed to drop slightly to pH 5 for all samples. To remove excess salts and unconsumed nutrients, the autoclaved mixtures (pellets and surrounding liquid) were dialyzed for 2 d under running deionized water

NC-Mycelium Co-Incubation: The co-incubated samples were prepared as described above for the fungal incubations, with one exception: the water in the liquid medium was replaced with NC suspensions of different concentrations, ranging from 0.2 to 2 wt%. These NC-containing mixtures were thoroughly combined by magnetic stirring prior to autoclaving to encourage the uniform dispersal of the NC.

Material Processing: To process into films or aerogels, the dialyzed liquid cultures (pellets and surrounding media) were homogenized using a Polytron PT 3100D model at 7500 rpm for 2 min. Aerogels were produced by lyophilization and films by vacuum filtration through membranes (Durapore membrane filters; 0.65 μm DVPP) of 0.1 wt% well-mixed slurries to achieve a target grammage of 30 g m $^{-2}$. Semidried films were carefully transferred to a frame for constrained drying to prevent shrinkage and wrinkling and were fully dried under controlled conditions (23 °C, 50% RH). Films were 8 cm in diameter and were ≈20 μm thick.

HR-SEM: An HR-SEM (Zeiss Ultra Plus, Germany), equipped with a Schottky field-emission electron gun and a Gemini electron-beam column design, was used. The microscope was operated at low acceleration voltages of 1.5–2 kV and working distances of 3.5–4.5 mm. Evart—Thornley secondary electron imaging detectors or high-resolution in-the-lens secondary electron detectors were used to acquire images. To improve electrical conductivity, samples were coated (Quorum, Q150TES, UK) with several nanometers of carbon, using short pulses of low evaporation current to prevent organic material degradation. Pellets produced through the various incubations were submerged in ethanol overnight to solvent exchange, followed by critical point drying (CPD). Using tweezers, dried pellet pieces were carefully transferred to SEM stubs covered with carbon tape for imaging.

Cryo-SEM: A Zeiss Ultra Plus high-resolution SEM, equipped with a Schottky field-emission gun and with a BalTec VCT100 cold-stage maintained below –145 °C, was used from cryo-SEM imaging. Specimens were imaged at low acceleration voltages of 1–1.4 kV and

working distances of 3.5–5 mm. Everhart–Thornley secondary electron imaging detectors were used. Low-dose imaging was applied to all specimens to minimize radiation damage. Specimens were prepared by placing a mycelium pellet into a cross-sectional stub, which was then immersed into liquid ethane at –183 °C and transferred into liquid nitrogen to be screwed into a specialized sample table. Next, the frozen sample was transferred into a BAF060 freeze fracture system, where the pellets were fractured using a rapid stroke from a cooled knife to expose their inner structure. Following the fracturing, the sample was transferred into the precooled HR-SEM for imaging as described above. Imaging was performed as close as possible to the pellet surface, where the cooling rate was maximal. If needed, gentle sample sublimation was done inside the microscope by rapidly increasing the stage temperature to –100 °C and then decreasing it back to the stage initial temperature.

POM: A Zeiss Axioplan polarized optical microscope equipped with a 540 nm waveplate was used to visualize the various materials produced in this study (NC, pellets, surrounding liquid, homogenized mixtures, films, and aerogels) and to contrast between the nonbirefringent hyphal network and birefringent NC.

AFM: I) AFM images of NC and of mycelium materials were collected under ambient conditions using a MultiMode 8 (Bruker, Santa Barbara, CA) in TappingMode with RTESP-150 cantilevers having a nominal resonant frequency of 150 kHz and a spring constant of 5 N m⁻¹, respectively. Mycelium samples were prepared by spin coating onto plasma-cleaned cleaved silica wafers. For anionic NC samples, wafers were first coated with PAH (0.1 wt%) followed by thorough rinsing. II) The average roughness (Ra) of hybrid films was obtained from topographical images of the samples measured in tapping mode with a Bruker FastScan AFM. Topography and nanomechanical measurements of the samples were carried out in PeakForce QNM method with a Bruker FastScan AFM using a Tap 300 DLC probe (BudgetSensors). The cantilever spring constant was calibrated using the thermal tune method and was 40 N m⁻¹. The actual tip outer radius was calibrated prior to measurements by conducting the elastic modulus mapping of a reference sample with known elasticity (polystyrene, PSfilm-12M, Bruker). The imaging setpoint in PeakForce QNM measurements was 75 nN and the obtained images contained 256 \times 256 data points. The DMT modulus was fitted to obtain the nanomechanical maps (obtained in PeakForce mode) used to calculate the average elastic moduli of the

 $\dot{\textit{XPS}}$: XPS spectra were recorded using a Kratos AXIS Ultra^{DLD} X-ray photoelectron spectrometer (Kratos Analytical, Manchester, UK). The samples were analyzed using a monochromatic Al X-ray source, at a depth of ≈10 nm and a lateral resolution of ≈1 mm², with most of the signal from an area of ≈700 × 300 μm. Survey spectra were run to detect elements present in the surface layer, and relative surface compositions (expressed in atomic %) were then obtained from quantification of detailed spectra run for each element detected. In addition, high-resolution carbon spectra were curve-fitted, showing chemical shifts in the carbon signals due to different functional groups.

ATR-FTIR: A Perkin Elmer Spectrum One FT-IR Spectrometer with ATR accessory and diamond ATR crystal was used to characterize the chemical signature of films produced from homogenized mixtures after fermentation and dialysis.

Tensile Testing of Films: Tensile properties were determined using an MTS ISA 3125, equipped with a 2 kN load cell. Films were cut into strips (6 mm wide \times 45 mm long) using a stamp and the average mass of a single strip was determined from the mass of 4 strips. Strips were clamped at 40 psi to give a 30 mm specimen length and extended at a rate of 5 mm min $^{-1}$ until breakage. The average tensile properties were reported for 6 film strips.

UV-Vis: UV-vis spectroscopy was conducted to assess turbidity/ stability by measuring absorbance at 550 nm as a function of time (0 and 12 h), with and without dilution. Liquids were placed into standard plastic cuvettes (10 mm path length) and absorbance was measured using a LAMBDA 265 UV/vis, with water used as a blank.

ADVANCED SUST AINABLE SYSTEMS

23667486, 2021, 2, Downloaded from https://onlinelibrary.wiley.com/doi/10.1002/adsu.202000196 by Epf1 Library Bibliothèque, Wiley Online Library on [08/12/2024]. See the Terms and Conditions (https://onlinelibrary.wiley.com/term

and-conditions) on Wiley Online Library for rules of use; OA articles are governed by the applicable Creative Commons License

Supporting Information

Supporting Information is available from the Wiley Online Library or from the author.

Acknowledgements

N.A. and T.A. contributed equally to this work. Y. Hadar is gratefully acknowledged for guidance and for commenting on the manuscript. O. Kleinerman, M. Sundin, S. Bardage, Å. Blademo, and Å. Engström are acknowledged for experimental support and discussion. The Technion Center for Electron Microscopy of Soft Matter (TCEMSM) and the Materials Engineering Electron Microscopy Center (MIKA) are acknowledged for facility access. The authors gratefully acknowledge funding from the Bo Rydin Foundation for Scientific Research. The acknowledgment to the Bo Rydin Foundation was added to the manuscript after initial publication, in February 2021.

Conflict of Interest

The authors declare no conflict of interest.

Keywords

biocomposite, cellulose nanocrystals, cellulose nanofibrils, mycelium, white-rot fungi

Received: August 19, 2020 Revised: October 18, 2020 Published online: November 25, 2020

- [1] K. Joshi, M. K. Meher, K. M. Poluri, ACS Appl. Bio Mater. 2020, 3, 1884.
- [2] M. A. Hubbe, A. Ferrer, P. Tyagi, Y. Yin, C. Salas, L. Pal, O. J. Rojas, BioResources 2017, 12, 2143.
- [3] M. Jones, T. Bhat, E. Kandare, A. Thomas, P. Joseph, C. Dekiwadia, R. Yuen, S. John, J. Ma, C. H. Wang, Sci. Rep. 2018, 8, 17583.
- [4] N. Lavoine, L. Bergström, J. Mater. Chem. A 2017, 5, 16105.
- [5] J. A. Whittaker, R. I. Johnson, T. J. A. Finnigan, S. V. Avery, P. S. Dyer, in *Grand Challenges in Fungal Biotechnology* (Ed: H. Nevalainen), Springer, Cham 2020, pp. 59–79.
- [6] D. Klemm, F. Kramer, S. Moritz, T. Lindström, M. Ankerfors, D. Gray, A. Dorris, Angew. Chem., Int. Ed. Engl. 2011, 50, 5438.
- [7] A. García, A. Gandini, J. Labidi, N. Belgacem, J. Bras, *Ind. Crops Prod.* 2016, 93, 26.
- [8] A. Isogai, J. Wood Sci. 2013, 59, 449.
- [9] M. S. Reid, M. Villalobos, E. D. Cranston, Langmuir 2017, 33, 1583.
- [10] O. Nechyporchuk, M. N. Belgacem, J. Bras, Ind. Crops Prod. 2016, 93, 2.
- [11] R. J. Moon, A. Martini, J. Nairn, J. Simonsen, J. Youngblood, Chem. Soc. Rev. 2011, 40, 3941.
- [12] A. Ferrer, L. Pal, M. Hubbe, Ind. Crops Prod. 2017, 95, 574.
- [13] F. V. W. Appels, S. Camere, M. Montalti, E. Karana, K. M. B. Jansen, J. Dijksterhuis, P. Krijgsheld, H. A. B. Wösten, *Mater. Des.* 2019, 161, 64.
- [14] N. Attias, O. Danai, T. Abitbol, E. Tarazi, N. Ezov, I. Pereman, Y. J. Grobman, J. Cleaner Prod. 2019, 246, 119037.
- [15] S. M. Bowman, S. J. Free, BioEssays 2006, 28, 799.
- [16] X. Kang, A. Kirui, A. Muszyński, M. C. D. Widanage, A. Chen, P. Azadi, P. Wang, F. Mentink-Vigier, T. Wang, *Nat. Commun.* 2018, 9, 2747.
- [17] The Fungi, 3rd ed. (Ed: L. Versteeg-Buschmann), Sara Tenney 2016 Elsevier Ltd., London 2016.

- [18] G. Xu, L. Wang, J. Liu, J. Wu, Appl. Surf. Sci. 2013, 280, 799.
- [19] R. A. Blanchette, Annu. Rev. Phytopathol. 1991, 29, 381.
- [20] A. D. Moreno, D. Ibarra, P. Alvira, E. Tomás-Pejó, M. Ballesteros, Crit. Rev. Biotechnol. 2015, 35, 342.
- [21] M. Papagianni, Biotechnol. Adv. 2004, 22, 189.
- [22] L. Veiter, V. Rajamanickam, C. Herwig, Appl. Microbiol. Biotechnol. 2018, 102, 2997.
- [23] P. A. Gibbs, R. J. Seviour, F. Schmid, *Crit. Rev. Biotechnol.* **2000**, *20*, 17
- [24] K. Bolla, B. V. Gopinath, S. Z. Shaheen, M. A. S. Charya, Int. J. Biotechnol. Mol. Biol. Res. 2010, 1, 15.
- [25] A. P. A. Tavares, M. S. M. Agapito, M. A. M. Coelho, J. A. Lopes Da Silva, A. Barros-Timmons, J. A. J. Coutinho, A. M. R. B. Xavier, World J. Microbiol. Biotechnol. 2005, 21, 1499.
- [26] Z. Ma, M. Xu, Q. Wang, F. Wang, H. Zheng, Z. Gu, Y. Li, G. Shi, Z. Ding, Front. Microbiol. 2019, 10, 2306.
- [27] H. A. B. Wösten, M. Van Wetter, L. G. Lugones, H. C. Van Der Mei, H. J. Busscher, J. G. H. Wessels, Curr. Biol. 1998, 3, 85.
- [28] M. Alfaro, A. Majcherczyk, U. Kües, L. Ramírez, A. G. Pisabarro, Sci. Rep. 2020, 10, 12421.
- [29] E. J. Okal, M. M. Aslam, J. K. Karanja, W. J. Nyimbo, Microb. Pathog. 2020, 147, 104410.
- [30] D. Grimm, H. A. B. Wösten, Appl. Microbiol. Biotechnol. 2018, 102, 7795
- [31] V. Meyer, Fungal Biol. Biotechnol. 2019, 6, 5.
- [32] F. V. W. Appels, J. Dijksterhuis, C. E. Lukasiewicz, K. M. B. Jansen, H. A. B. Wösten, P. Krijgsheld, Sci. Rep. 2018, 8, 4703.
- [33] M. Haneef, L. Ceseracciu, C. Canale, I. S. Bayer, J. A. Heredia-Guerrero, A. Athanassiou, Sci. Rep. 2017, 7, 41292.
- [34] W. M. F. W. Nawawi, M. P. Jones, E. Kontturi, A. Mautner, A. Bismarck, Compos. Sci. Technol. 2020, 198, 108327.
- [35] M. Jones, K. Weiland, M. Kujundzic, J. Theiner, H. Kählig, E. Kontturi, S. John, A. Bismarck, A. Mautner, *Biomacromolecules* 2019, 20, 3513.
- [36] F. V. W. Appels, J. G. van den Brandhof, J. Dijksterhuis, G. W. de Kort, H. A. B. Wösten, Commun. Biol. 2020, 3, 334.
- [37] W. Sun, M. Tajvidi, C. G. Hunt, G. Mcintyre, D. J. Gardner, Sci. Rep. 2019, 9, 3766.
- [38] K. Weiland, M. Jones, M. Fortea-Verdejo, A. Mautner, A. Bismarck, S. John, presented at 22nd Int. Conf. on Composite Materials, Melbourne, Australia, August 2019.
- [39] J. Ruiz-Herrera, L. Ortiz-Castellanos, Cell Surf. 2019, 5, 100022.
- [40] M. P. Jones, A. C. Lawrie, T. T. Huynh, P. D. Morrison, A. Mautner, A. Bismarck, S. John, *Process Biochem.* 2019, 80, 95.
- [41] L. Sabantina, F. Kinzel, T. Hauser, A. Többer, M. Klöcker, C. Döpke, R. Böttjer, D. Wehlage, A. Rattenholl, A. Ehrmann, *Nanomaterials* 2019, 9, 475
- [42] M. Haneef, L. Ceseracciu, C. Canale, I. S. Bayer, J. A. Heredia-Guerrero, A. Athanassiou, Sci. Rep. 2017, 7, 41292.
- [43] A. I. Puertas, M. T. Dueñas, C. Marieta, Fibers 2014, 2, 255.
- [44] M. Osińska-Jaroszuk, A. Jarosz-Wilkołazka, J. Jaroszuk-Ściseł, K. Szałapata, A. Nowak, M. Jaszek, E. Ozimek, M. Majewska, World J. Microbiol. Biotechnol. 2015, 31, 1823.
- [45] K. D. Hyde, J. Xu, S. Rapior, R. Jeewon, S. Lumyong, A. G. T. Niego, P. D. Abeywickrama, J. V. S. Aluthmuhandiram, R. S. Brahamanage, S. Brooks, A. Chaiyasen, K. W. T. Chethana, P. Chomnunti, C. Chepkirui, B. Chuankid, N. I. de Silva, M. Doilom, C. Faulds, E. Gentekaki, V. Gopalan, P. Kakumyan, D. Harishchandra, H. Hemachandran, S. Hongsanan, A. Karunarathna, S. C. Karunarathna, S. Khan, J. Kumla, R. S. Jayawardena, J.-K. Liu, N. Liu, T. Luangharn, A. P. G. Macabeo, D. S. Marasinghe, D. Meeks, P. E. Mortimer, P. Mueller, S. Nadir, K. N. Nataraja, S. Nontachaiyapoom, M. O'Brien, W. Penkhrue, C. Phukhamsakda, U. S. Ramanan, A. R. Rathnayaka, R. B. Sadaba, B. Sandargo, B. C. Samarakoon, D. S. Tennakoon, R. Siva, W. Sriprom,





www.advancedsciencenews.com www.advsustainsys.com

- T. S. Suryanarayanan, K. Sujarit, N. Suwannarach, T. Suwunwong, B. Thongbai, N. Thongklang, D. Wei, S. N. Wijesinghe, J. Winiski, J. Yan, E. Yasanthika, M. Stadler, *Fungal Diversity* **2019**, *97*, 1.
- [46] A. Livne, S. C. Mijowska, I. Polishchuk, W. Mashikoane, A. Katsman, B. Pokroy, J. Mater. Chem. B 2019, 7, 5725.
- [47] N. Vigneshwaran, A. A. Kathe, P. V. Varadarajan, R. P. Nachane, R. H. Balasubramanya, Colloids Surf., B 2006, 53, 55.
- [48] M. A. Prusinkiewicz, F. Farazkhorasani, J. J. Dynes, J. Wang, K. M. Gough, S. G. W. Kaminskyj, Analyst 2012, 137, 4934.
- [49] P. Baldrian, V. Valášková, FEMS Microbiol. Rev. 2008, 32, 501.
- [50] E. Gaulin, A. Jauneau, F. Villalba, M. Rickauer, M. T. Esquerré-Tugayé, A. Bottin, J. Cell Sci. 2002, 115, 4565.
- [51] R. Verker, A. Rivkin, G. Zilberman, O. Shoseyov, Cellulose 2014, 21, 4369.

- [52] A. Rivkin, T. Abitbol, Y. Nevo, R. Verker, S. Lapidot, A. Komarov, S. C. Veldhuis, G. Zilberman, M. Reches, E. D. Cranston, O. Shoseyov, *Ind. Biotechnol.* 2015, 11, 44.
- [53] S. Meirovitch, Z. Shtein, T. Ben-Shalom, S. Lapidot, C. Tamburu, X. Hu, J. Kluge, U. Raviv, D. Kaplan, O. Shoseyov, *Int. J. Mol. Sci.* 2016, 17, 1573.
- [54] M. Jones, T. Huynh, C. Dekiwadia, F. Daver, S. John, J. Bionanosci. 2017, 11, 241.
- [55] C. Girometta, A. M. Picco, R. M. Baiguera, D. Dondi, S. Babbini, M. Cartabia, M. Pellegrini, E. Savino, Sustainability 2019, 11, 281.
- [56] L. Wågberg, G. Decher, M. Norgren, T. Lindström, M. Ankerfors, K. Axnäs, *Langmuir* 2008, 24, 784.
- [57] M. Henriksson, G. Henriksson, L. A. Berglund, T. Lindström, Eur. Polym. J. 2007, 43, 3434.